LAWRENCE
LIVERMORE
NATIONAL
LABORATORY

LLNL-TR-656107

Using Computed Tomography to Non-Destructively Characterize Glassy Fallout in 3-D

R. Tapia, J. Sain, K. Knight, B. Isselhardt

June 24, 2014

Disclaimer

This work performed under the auspices of the U.S. Department of Energy by Lawrence Livermore National Laboratory under Contract DE-AC52-07NA27344.

Using Computed Tomography to Non-Destructively Characterize Glassy Fallout in 3-D

Rodrigo Tapia[1]; John Sain[2]; Kim Knight,[2]; Brett Isselhardt,[2]

[1]*University of Georgia, GA 30602, USA*
[2] *Lawrence Livermore National Laboratory (LLNL), CA 94551, USA*

Fallout glasses are one type of debris formed from the interaction of soil and surrounding materials with a nuclear explosion. During this interaction anthropogenic actinides and other components of the device are incorporated into the glassy fallout matrix. The rapid quenching of the melt glasses traps these materials and forms vesicles the fallout degases its volatilized materials. These inclusions and vesicles provide a snapshot of the conditions of the fireball and soil interactions. The vesicles are a common feature in fallout, but it has yet to be fully understood. Fallout has conventionally been studied by the detection of fission products, activation products, and remnant fuel through gamma spectrometry and mass spectrometry (1,2,3). Recent studies also explore how this residual activity is incorporated into these glassy materials. The distribution of structural materials and remnant fuel in these glasses can provide insights into fallout formation mechanisms (1,4,5). These inclusions, if not fully diffused, have markedly different densities than that of the silicate glass found in fallout. Characterization of these features is possible with density contrast techniques such as computed tomography (CT). Likewise, the preservation of void spaces in these materials can be quantified across populations of samples using the spatial resolution of tomography. These techniques have the additional benefit of being non-destructive, allowing for subsequent analyses such as the conventional methods listed above.

This project investigated the application of X-ray CT for characterizing fallout glasses. The project is divided into two main efforts: 1) exploration of the compositional makeup of fallout glasses through density mapping and 2) the quantification of fallout porosity and gas evolution features. We developed an analytical approach to use CT images to non-destructively characterize the density and structure of individual mm- to cm-sized pieces of glassy fallout. The CT system used here is a conventional micro CT instrument, capable of resolution on the order of 10 microns, which enables non-destructive characterization of spatially resolved density and compositional features within fallout. We report our methods and preliminary observations here.

In addition to non-destructive imaging of the fallout samples, several reference metals were analyzed by CT in this study. This was done to gain insight into the possible composition of observed areas of high density in the glasses. Among the metals analyzed were three samples of indium, one of cobalt, and one of aluminum (material densities of 7.31 g/cm^3, 8.90 g/cm^3, and 2.70 g/cm^3, respectively).

X-ray computed tomography is a method of three-dimensional (3-D) imaging based upon the attenuation of radiation, that is, the absorption and scattering of radiation by a material that results in the diminished transmission of the incident radiation through the material. An X-ray source directs radiation through the sample, and this radiation is attenuated by the sample. The extent of attenuation is proportional to the average electron density of the material that is being irradiated, such that the higher the average electron density, the greater the attenuation. This property of average electron density roughly corresponds to both atomic number (Z) and material density, thus the resultant images reflect a combination of a material's chemical composition and structure.

Attenuation of radiation tends to increase as photon energy decreases with all else being constant. Since the X-ray sources used here emit a broad Brehmsstrahlung spectrum of energies, the lower energy photons are more readily attenuated, allowing the X-rays of higher energy to be preferentially transmitted. The difference in energy spectra for the X-ray beams incident upon and being transmitted through the object of interest is the result of a physical phenomenon known as beam hardening, and it can interfere with accurate reconstruction of the CT data set. This effect can be minimized by selecting an X-ray energy range appropriate to the material of interest or in some cases, by pre-filtering of the beam (6,7).

2. Methods

2.1 Samples and preparation

A total of eight pieces of black-colored and mm- to cm-sized glassy fallout were isolated from soil collected near the location of a historical nuclear test (1), and were imaged by CT under two different

sets of conditions. The fallout is described as one of two morphologies: aerodynamic or irregular (5). Aerodynamic samples are glasses that have smooth surfaces and are simple in shape – often tending to be nearly spheroidal but also occasionally oblong in shape like a capsule or a raindrop. Irregular samples are defined as being more complex in morphology, often preserving multiple agglomerations of smaller, aerodynamic objects that came into contact while molten, and/or containing textural heterogeneity observable by eye or optical microscope such as small rocky inclusions (see Fig. 1).

The samples were mounted for X-ray computed tomography in two ways. The first set of samples (numbers 1, 6, 7) was placed inside a polycarbonate tube with foam to hinder sample movement or vibration during data collection. The tube was sealed with a polycarbonate plug and was attached to the top of a metal sample pin-type mount using epoxy (Fig. 2). The foam was found to deform slightly during irradiation, compromising the quality of the resultant images to some degree. Thus a second set of sample holders utilized solid plastic spacers instead of the foam to control sample movement and position during data collection. Some of these latter holders contained more than one sample, or a sample and a reference metal, separated by spacers. These reference metal samples were prepared as disks with approximate thicknesses of 1 mm and radii of 2 mm.

2.2 Instrumentation

The X-ray computed tomography data sets were obtained using an Xradia MicroXCT-200 system at Lawrence Livermore National Laboratory. A 150-kV Hamamatsu L8121-03 X-ray source was used with a two-stage detector, a CsI scintillation crystal optically coupled to an Andor iKon 2K x 2K CCD camera via a 4X microscope objective and turn mirror. The data sets were reconstructed using the Feldkamp method, which uses a convolution-backprojection formula to reconstruct a three-dimensional density map (8). The CCD detector pixel sizes in the resulting images range from 1.7 - 2.8 μm. The sets of data analyzed for density comparisons and inter-comparisons were all collected under similar conditions with a Brehmsstrahlung X-ray spectrum of maximum energy 150-kV. The data set for a given sample is comprised of many two-dimensional, grayscale images that form the three-dimensional object. These grayscale images were useful in quantifying void space, however the intensities are normalized in each image, so for density calculations the raw data was used (.SDT file format).

2.3 Image processing: Density analysis

The fallout samples have an average material density of 2.35 g/cm^3, calculated in this study by using recorded masses and values of volume found from the image processing of the spatially resolved CT data. These samples contain inclusions and heterogeneities, which differ in density from the glass. These regions of fallout glasses with higher intensity relative to the bulk composition (in the convention used here, higher intensity corresponds to higher attenuation), hereafter referred to as hotspots, were located manually by inspection of the grayscale images of the samples. The image processing for density analysis required the use of the raw data, since the grayscale image intensity of each image is individually scaled between 1 - 256, impeding any comparison between images. The raw intensities were collected for manually selected areas of interest.

In Figs. 3a and 3b, the intensity data from the fallout and metal samples are described in order to identify similarities as well as to determine the presence and impact of beam hardening on the resultant data. For each sample, this data represents the raw intensities of five adjacent rows of pixels averaged together in order to minimize noise. In Fig. 3a it is important to note that the intensity maps of the denser metals appear depressed toward the center of the materials due to a beam hardening artifact (see section 1.2) known as ‘cupping’ (6,7). The effects of beam hardening are most significant in the images of the indium sample, where this effect causes a relatively steep drop in signal intensity towards the center of the sample. In Fig. 3b it is shown that the glassy fallout materials, all have highly similar intensities (standard deviation of ± 2.41% intensity). There do not appear to be any significant complications from beam hardening among the fallout samples. In the data from aluminum metal, there is only a slight cupping artifact is evident.

The reference metals were mounted alongside fallout samples and were co-irradiated during the CT data acquisition. The intention of including these reference metals was to provide a basis for calibration of sample density. However, the accuracy of such a linear calibration is low in this study, due to the increased effect of beam hardening with increasing material density. Nonetheless, by making several assumptions, a first-order approximation of density is possible.

2.4 Image processing: Void space analysis

The volume and frequency of void spaces in the fallout glasses were characterized by applying a binary thresholding algorithm to each 2-D slice

throughout the 3-D reconstruction. Typically each 3-D stack is composed of ~1500 2-D slices. The grayscale image of the object was converted to a binary image based on a global threshold determined by Otsu's method, which returns an image with values of 0 assigned for all areas outside of the object as well as for the void areas within the object (9). In order to minimize the impact of noise or phantom objects with values of 1, all connected pixel areas that were smaller than the manually determined size, typically 100 - 250 pixels in area, were removed by creating a new image without these data. This size was chosen because smaller limits tended to include large amounts of noise from the image. The binary image was then inverted, assigning 1's to void areas. A silhouette of the first binary object was created separately, and then multiplied by the inverted binary image, resulting in an image with values of 1 assigned only to the voids within the sample (thus excluding voids outside of the sample). Fig. 4 shows a visual representation of the image processing procedure.

Once the void areas were isolated in the image using this threshold-based algorithm, groups of connected components (void bodies) were labeled with a value of 1, and their areas were recorded. The areas of the 2-D sample silhouettes were calculated similarly, frame by frame. By subtracting the total void area from the total silhouette area of the sample, the non-void area of the object was determined. This process was then iterated over all frames that made up the 3-D reconstruction of the sample.

In order to obtain information about each of the individual void volumes, further calculations were required. Once the 2-D void bodies were identified in each frame, their area and centroid location were reported. This information was used, with no assumptions about the morphology of the void space, to associate the groups of 2-D void areas that comprised each 3-D void object. Two void areas were considered to be part of the same void volume if they satisfied two criteria: 1) the two void areas appeared in adjacent frames and, 2) the centroid of the smaller body was located within one half of the radius of the larger body. The latter criterion provided a specific method to distinguish between individual voids.

3. Results and discussion

3.1 Density Analysis

The average intensities of the fallout samples are highly similar to that of the aluminum metal (the densities of aluminum and fallout are 2.7 g/cm^3 and 2.35 g/cm^3 respectively). There is a 5.7% difference in average intensity between the fallout and aluminum, calculated from the averaged raw intensity values from the CT data of the samples, which is consistent with the general similarities in density of the two materials (13.5% difference in material density). The average intensities of indium and cobalt respectively, were factors of 13.3 and 8.4 higher than that of the fallout. While the average intensities reflect the expected trend of attenuation with increasing average electron density, these reference metal samples exhibit substantial beam hardening artifacts and the relative standard deviation between the four indium samples is 29%. This high level of deviation can be explained by the differing sizes and morphologies of the indium samples, which can affect the extent of beam hardening. See Table 1 for detailed description of the intensity data.

An initial intention of this study was to compare the intensities of the reference metals to areas of similarly high attenuation in the fallout samples and quantify the material density of the regions of interest. It is necessary to assume the X-ray beam is pseudo-mono-energetic such that there is no beam hardening, though in reality the beam used has a Bremsstrahlung energy spectrum and hardening is observed. Although the accuracy of this sort of calculation is low given the experimental set-up in this study, a useful approximation can be found. In Sample 1, two regions were found and quantified, an area of higher intensity and one of lower intensity relative to the average glass. These areas of interest in Sample 1 were calculated to have densities of 1.97 and 5.26 g/cm^3. The former could represent a mineral inclusion of lower density than the silicate matrix, and the latter matches very well with the density of iron (III) oxide (5.24 g/cm^3), which can reasonably be expected to exist in the fallout. These values were calculated by calibrating against the intensities and known densities of bulk fallout, aluminum, and cobalt. These standards span a wide range of densities (2.35 – 8.9 g/cm^3), with a large gap between the aluminum and cobalt standards. Future studies with optimized CT parameters and a more comprehensive set of standards could improve the accuracy significantly of these calculations substantially.

3.2 Void Analysis

The image processing method described in section *2.4* was used to carry out the void analysis of samples 1 – 6. Overall sample volume and individual void volume data were collected for each sample and are reported in Figs. 5a, 5b and Table 2 (Sample 6 is excluded from Figures 5a and 5b because the quality of its data was insufficient for sensitive analysis). A threshold volume of 5500 μm^3 (corresponding to a sphere of radius ~10 μm) was

set as a minimum void size in order to mitigate the occurrence of false voids due to limits of spatial resolution. No voids smaller than this volume were considered. This threshold could be lowered for images with less noise.

Void volumes are very small compared to the total volumes of the samples. The average combined volume of all voids in a sample is 2.2% of the total sample volume. On average, the volume of a single void in a sample makes up only 0.0172% of the total sample volume. The total number of voids in these samples ranges from 51 – 468, and no relationship is observed between number of voids in a sample and the average volume of a single void. See Table 2 for more detailed statistics.

The distributions of individual void volumes are similar between the samples (Fig. 5a and 5b). There are a large number of small voids with negligible volumes ($<2.20 \times 10^5$ μm^3 or ~0.0005%), and a small number of larger voids, the latter contributing to the majority of the void volume in a given sample. Though sample 5 shows this same trend in void volume distribution (Fig. 5b), the total void volume is 7.8% of the sample, compared to the average value of 2.2%. Samples 1 - 4 are similar to each other in void volumes and relative statistics (Table 2), but sample 5 contains a much greater void volume. The largest void in sample 5 is two orders of magnitude larger than any single void observed in other samples.

The approaches demonstrated here could be applied to a larger number of samples to more accurately represent the statistical distributions of void volumes in these fallout materials. These statistical distributions could in turn help illuminate the conditions and time, temperature history of formation of the samples. Outside of nuclear forensics, fields such as volcanology have used bubble size distributions to inform degassing models for explosive volcanic eruptions (10). The modeling of fallout formation is key to the development of accurate nuclear forensics in a post-detonation scenario.

4. Conclusion

Our results demonstrate that CT is capable of spatially resolving high density (inclusions) and low-density (inclusions and void space) features in fallout on the order of 10 microns. Using CT we can identify both the size and location of these features in fallout. Beam hardening does not significantly impact relative signal intensity for fallout samples. Standard materials have been included in these CT analyses to aid in calibration of the relative attenuation of photons, but the effects of beam hardening were too great to allow for accurate calibration. With further study and calibrated standards it may be possible to apply this method to quantitatively constrain the average and spatially resolved material densities of fallout, including compositional inclusions. Present quantification of the composition of high and low-density features, however, requires additional post-CT image analytical techniques. Alternatively, careful pre-filtering of the beam by a thin sheet of material such as Al or Cu could reduce the effects of beam hardening (6,7).

CT and image post-processing can quantify void volumes and their statistical distributions in glassy fallout. While outside the scope of this exploratory study, such information can be used to help constrain the time-temperature history of a sample when paired with compositional information and a model for silicate melt viscosities.

This study serves as a proof-of-principle effort for the use of CT for non-destructive fallout characterization. We have also shown that CT can serve as an effective tool to guide destructive and/or spatially resolved fallout analyses. Once the sample density has been mapped through CT, for example, the sample is fully recoverable, and regions of interest could be efficiently targeted and isolated for additional analysis. With improved calibration and automation of image processing, CT can provide rapid assessment of the internal structure of fallout materials. In order to accurately characterize populations of fallout, a streamlined and fully automated method for data collection and data processing is required.

Acknowledgements

This research was performed under the Nuclear Forensics Undergraduate Scholarship Program, which is sponsored by the U.S. Department of Homeland Security Domestic Nuclear Detection. Office. We thank the U.S. Department of Energy's National Nuclear Security Administration, Office of Defense Nuclear Nonproliferation Research and Development, for financial support. This work performed under the auspices of the U.S. Department of Energy by Lawrence Livermore National Laboratory under Contract DE-AC52-07NA27344. LLNL-TR-656107.

References

1. Eppich GR, Knight KB, Jacomb-Hood TW, Spriggs GD, Hutcheon ID. Constraints on fallout melt glass formation from a near-surface nuclear test. J Radioanal Nucl Chem 2014;302:593-609.

2. Parekh PP, Semkow TM, Torres MA, Haines DK, Cooper JM, Rosenberg PM, Kitto ME. Radioactivity in Trinitite six decades later. J Environ Radioactiv 2006;85(1):103-20.

3. Bellucci JJ, Simonetti A, Wallace C, Koeman EC, Burns PC. Isotopic fingerprinting of the world's first nuclear device using post-detonation materials. Anal Chem 2013;85(8):4195-8.

4. Cassata WS, Prussin SG, Knight KB, Hutcheon ID, Isselhardt BH, Renne PR. When the dust settles: stable xenon isotope ratio constraints on the formation of nuclear fallout. J Environ Radioactiv 2014;137:88-95.

5. Lewis L, Knight K, Matzel J, Prussin S, Zimmer M, Kinman W, Ryerson F, Hutcheon I. Spatially-resolved analyses of aerodynamic fallout from a uranium-fueled nuclear test. J Environ Radioactiv 2015;148:183-95.

6. Meganck JA, Kozloff KM, Thornton MM, Broski SM, Goldstein SA. Beam hardening artifacts in micro-computed tomography scanning can be reduced by X-ray beam filtration and the resulting images can be used to accurately measure BMD. Bone 2009;45(6):1104-16.

7. Brooks RA, Chiro GD. Beam hardening in X-ray reconstructive tomography. Phys Med Biol 1976;21(3):390-8.

8. Feldkamp LA, Davis LC, Kress JW. Practical cone-beam algorithm. J Opt Soc Am A 1984; 1(6):612-9.

9. Otsu N. A threshold selection method from gray-level histograms. IEEE Trans Syst Man Cybern 1979;9(1):62-6.

10. Blower JD, Keating JP, Mader HM, Phillips JC. The evolution of bubble size distributions in volcanic eruptions. J Volcanol Geoth Res 2003;120:1-23.

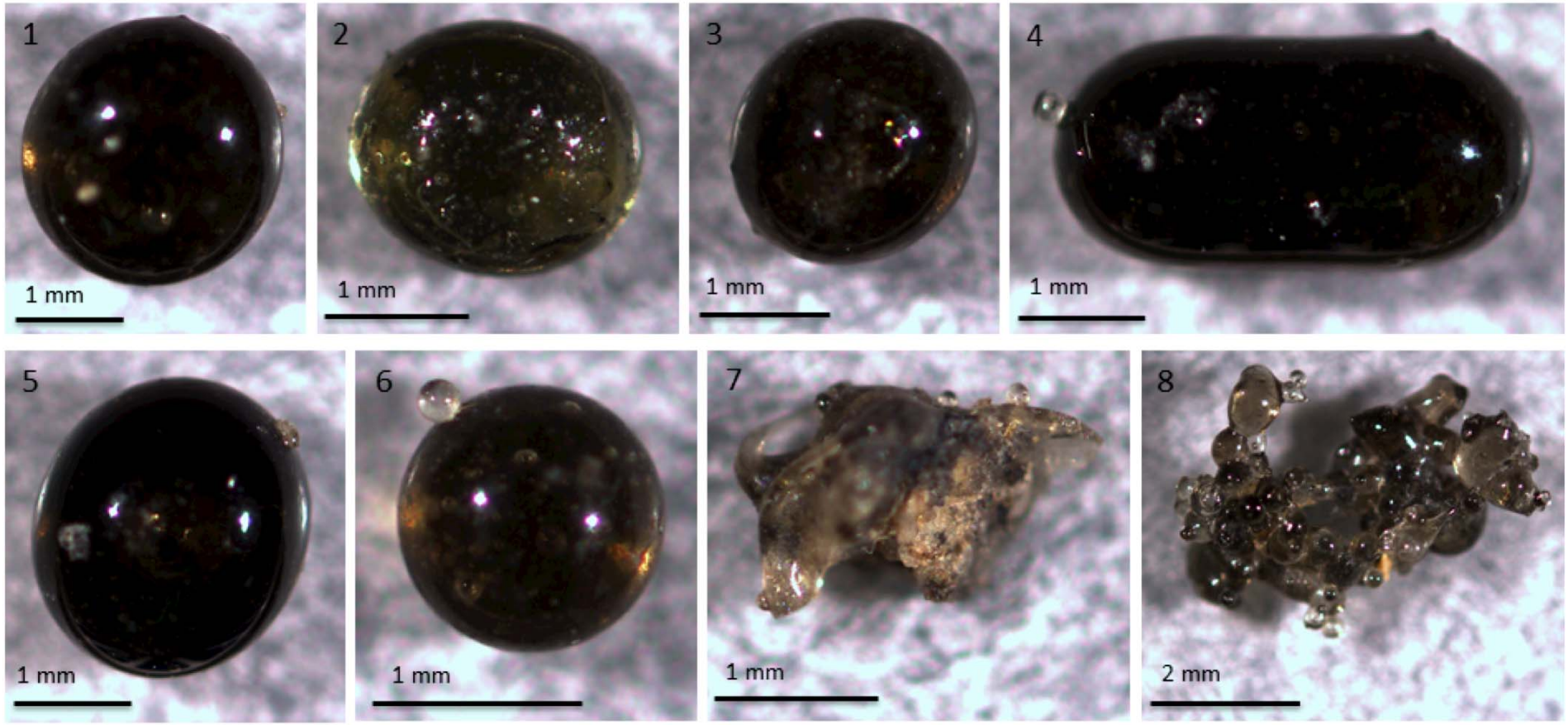

FIG. 1—Samples 1 - 8

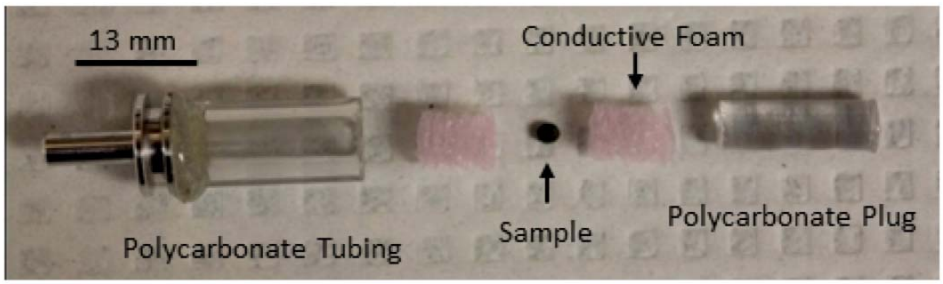

FIG. 2—Sample mounts used in initial CT data collection.
Top: Disassembled
Bottom: Assembled

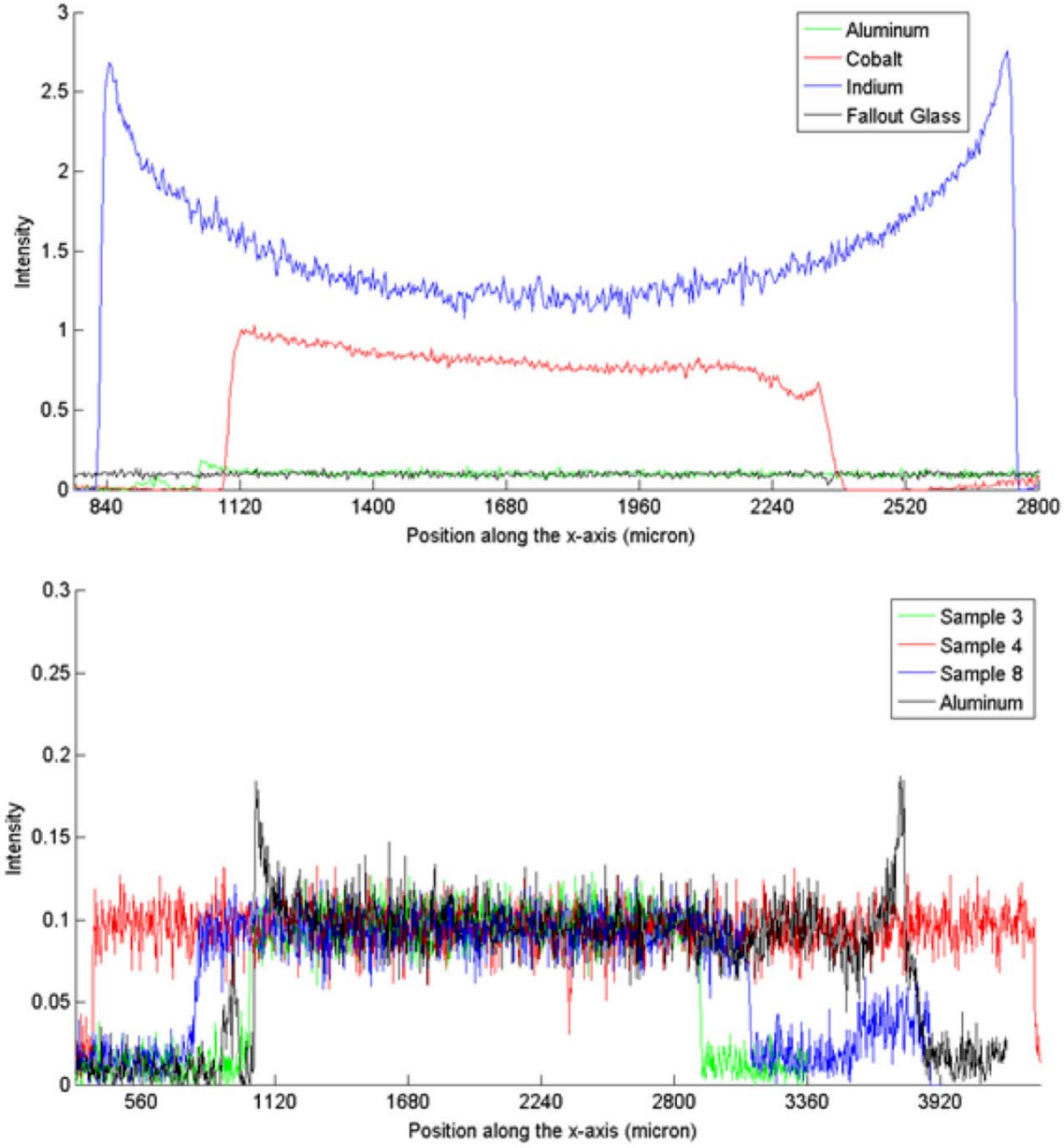

FIG. 3a (top) and 3b (bottom)—CT intensity data of several samples plotted along the x-axis. The cupping effects of beam hardening can be seen where the intensity spikes at the edges of the material and decreases towards the center.

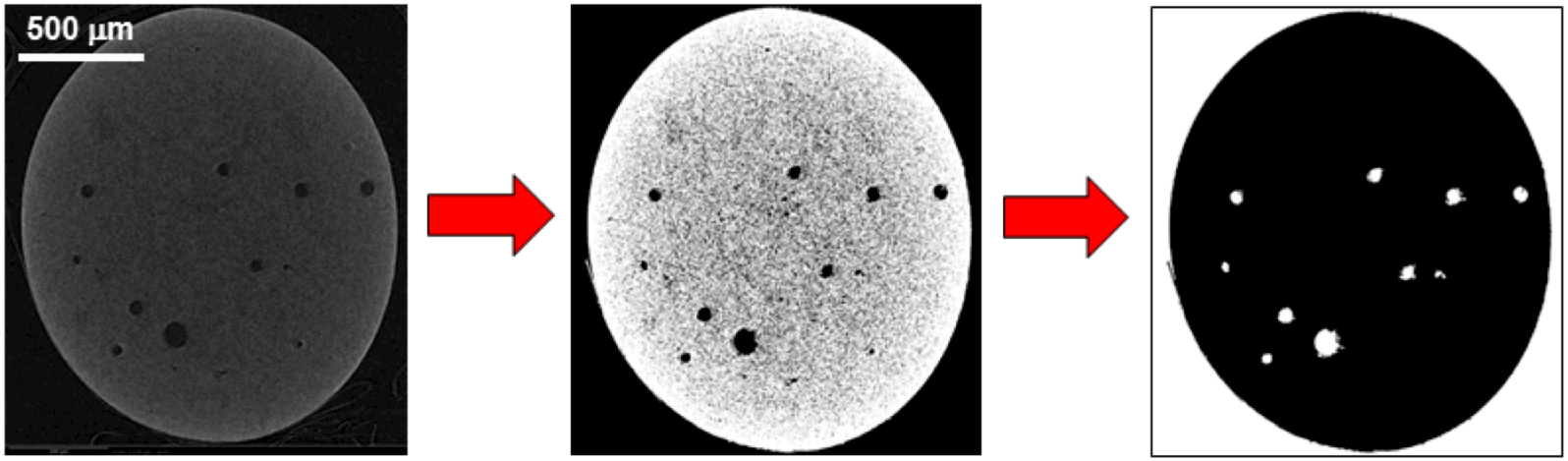

FIG. 4—Demonstration of image processing method for void analysis. Original image (left) is converted to binary by thresholding and the subsequent binary image (center) is isolated for the voids by removing the noise (right).

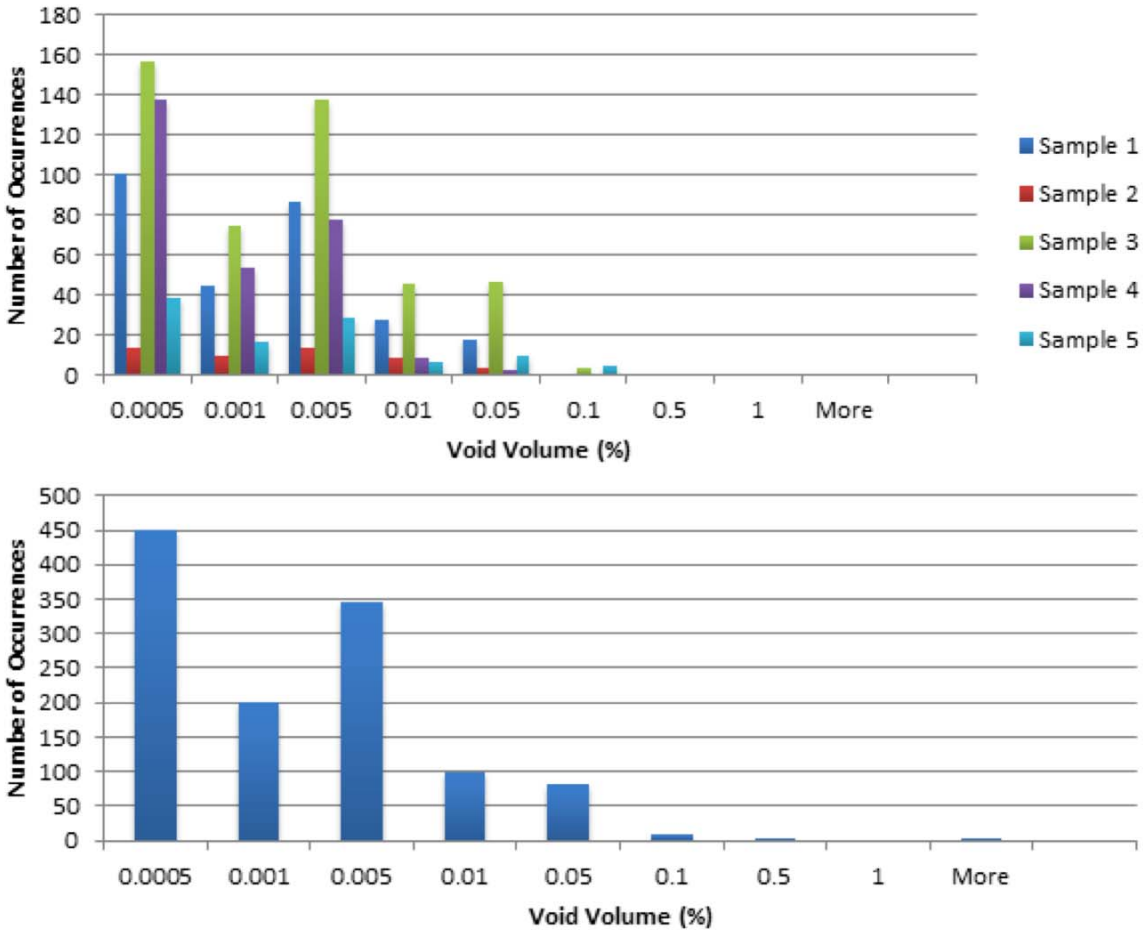

FIG. 5a (top) and 5b (bottom)—Distribution of individual void sizes for different samples (5a) and distribution of void sizes across all samples (5b). All void volumes are listed as a percentage of the total volume of their respective sample.

Table 1: Intensity of reference metals and fallout glasses.

	Material	Max Intensity	Average Intensity
Sample Set 1	Indium	2.8846	1.5876
	Glass	0.1288	0.093
Sample Set 2	Indium	2.409	1.0828
	Glass	0.1289	0.0976
Sample Set 3	Indium	2.0666	0.8865
	Glass	0.1325	0.0955
Sample Set 4	Indium	2.7579	1.5108
	Aluminum	0.1841	0.101
	Cobalt	1.0295	0.8033

Table 2: Sample characteristics and void volumes (NM = not measured)

	Sample 1	Sample 2	Sample 3	Sample 4	Sample 5	Sample 6	Sample 7	Sample 8
Morphology	Irregular	Aero-dynamic	Aero-dynamic	Aero-dynamic	Aero-dynamic	Irregular	Irregular	Irregular
Mass (g)	0.0149	0.0073	0.008	0.0193	0.0161	0.0024	0.0021	0.0165
Counts/ Min (β)	198	63	147	378	318	66	22	315
Calculated Volume (mm^3)	6.33	3.13	3.55	8.29	7.46	1.00	NM	NM
# of Voids	280	51	468	282	108	280	NM	NM
Total Void Volume (%)	0.8970	0.1704	1.9743	0.3233	9.5561	0.6101	NM	NM
Average Volume of a single void (%)	0.0032	0.0033	0.0042	0.0011	0.0885	0.0022	NM	NM
Volume of Largest Void (%)	0.1081	0.0174	0.1595	0.0193	8.8632	0.0593	NM	NM
Material Density (g/cm^3)	2.375	2.336	2.299	2.336	2.386	2.415	NM	NM